In Vitro PET Imaging of a Miniature Ventricular Assist Device

Michael S. Gossman[1], Joel D. Graham[2], Stephen Depot[2], Huaiyu Zheng[3], Junling Li[3], Chin K. Ng[3], and Daniel Tamez[2]

[1]Regulation Directive Medical Physics, Russell, Kentucky; [2]HeartWare, Inc., Miami Lakes, Florida; and [3]Department of Radiology, University of Louisville School of Medicine, Louisville, Kentucky

Interactions between the life-sustaining ventricular assist devices and diagnostic therapies must be carefully considered to decrease the risk of inaccurate diagnostic imaging or pump failure. **Methods:** The MVAD® pump, currently under investigational use, was tested for interaction with radiotracers in an in vitro flow-loop study. The radiotracers ^{18}F-sodium fluoride and ^{18}F-FDG were injected into a closed loop to determine the feasibility of direct imaging of the MVAD® pump in a PET scanner. **Results:** No real-time changes were observed in pump operation, and there were no statistical differences in pump parameters (power consumption, speed, and estimated flow rate) between the baseline and circulation conditions. In addition, no effect was observed on any external components, including the permissive-action-link controller and the batteries powering the device. Imaging of the internal pump components was possible, with obscuration observed only in the portion of the pump where the spinning impeller is located. Retention of radiotracer in the pump components after circulation was minimal (<1%). **Conclusion:** PET imaging is an attractive diagnostic tool for patients with a ventricular assist device and may have additional utility outside its current use, detection of infection.

Key Words: MVAD®; PET; pump; radioactive; ventricular assist device

J Nucl Med Technol 2016; 44:190–194
DOI: 10.2967/jnmt.116.175885

The use of a ventricular assist device (VAD) in patients with severe heart failure is increasing because of the lengthy wait for heart donors (*1–4*). As a result, VADs have been used as a bridge until a heart transplant becomes available or as a destination therapy (*5–7*). The MVAD® pump (currently for investigational use only; HeartWare®, Inc.) is a mechanical assist device with continuous, axial blood flow (*5,8*). The miniaturized design allows implantation in smaller patients, as well as allowing a potentially shorter hospital stay through use of less invasive surgery such as a thoracotomy (*9,10*). The design of the pump includes a wear-free impeller suspended in a motor core though passive magnetic and hydrodynamic forces rotating at 8,000–18,000 rpm. The primary aim of this study was to assess the effect of PET imaging on operation of the pump. Secondary aims were to detect potential scattering and attenuation in the images and to determine the level of γ-radiation retained in the pump. Figure 1 portrays the surgical position of the MVAD® pump relative to the anatomy of the heart. The directional flow of pumped blood can be immediately visualized.

PET is a noninvasive nuclear imaging procedure commonly used to detect cancer and heart disease. The PET system detects pairs of γ-rays emitted indirectly by a positron-emitting radionuclide introduced into the body on a biologically active molecule. Three-dimensional (3D) tomographic images of radiotracer concentration are constructed by computer analysis. The radionuclides that are used in PET scans are called contrast agents. These are typically isotopes with short half-lives, such as ^{13}N (10 min) and ^{18}F (110 min). When these contrast agents are incorporated into compounds normally used by the body, such as glucose, they are known as radiotracers. PET technology traces the biologic pathway of compounds in vivo, providing quantitative parameters on cell viability, cell proliferation, and the metabolic activity of tissue. Two commonly used radiotracers in clinical scanning are ^{18}F-FDG and ^{18}F-NaF. The use of ^{18}F-FDG is, internationally, primarily oncologic. ^{18}F-NaF is commonly used for detecting and evaluating metastatic bone cancer (*11,12*).

In the clinical setting, there is concern about scattering or attenuation of x-rays during imaging because of the metallic components of ventricular assist devices. Another concern is that after injection of the radiopharmaceutical, radioactivity may be retained in the MVAD® pump instead of being circulated to biologic tissue. Imaging artifacts may result, with the consequent poor contrast and resolution potentially leading to an error in diagnosis. The reported uses of PET imaging in the VAD patient population have been limited to detection of infection (*1,13–15*). In this study, we examined the effect of PET imaging on the MVAD® pump, using an in vitro flow loop with two commonly applied radiopharmaceuticals, ^{18}F-NaF and ^{18}F-FDG.

MATERIALS AND METHODS

An MVAD® pump with an attached 10 mm outflow graft (Vascutek) was connected to a 1.2 L in vitro flow loop filled with deionized water and glycerin at a 2:1 ratio. The system

Received Mar. 22, 2016; revision accepted May 4, 2016.
For correspondence or reprints contact: Michael S. Gossman, Regulation Directive Medical Physics, 104 Hildeen Ct., Russell, KY 41169.
E-mail: msgossman@hotmail.com
Published online Jun. 30, 2016.

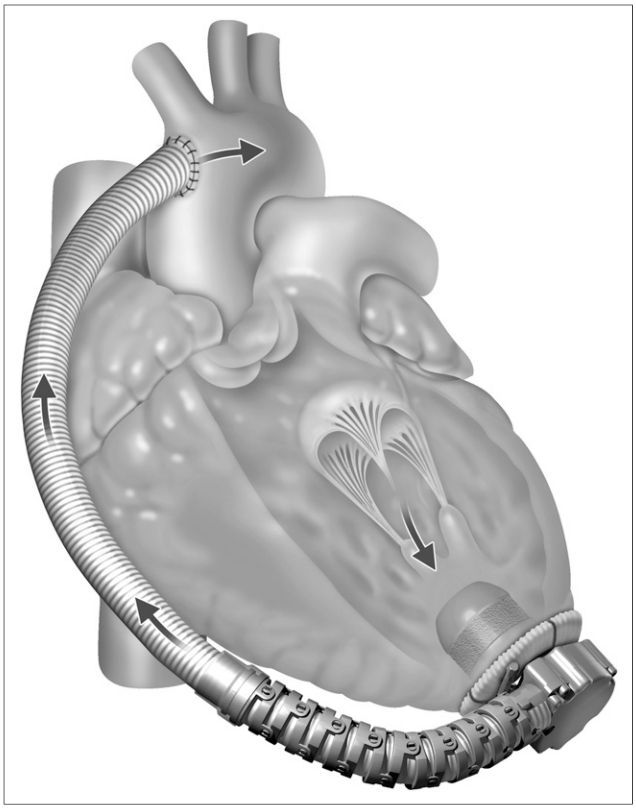

FIGURE 1. MVAD® surgically attached to heart. (A color version of each of the 6 figures is available as a supplemental file at http://tech.snmjournals.org.)

components include an external permissive-action-link controller (PAL®; HeartWare®, Inc.) that connects to a percutaneous driveshaft, an alternating-current adaptor, and a battery. The controller manages power, monitors pump function, provides diagnostic information, and stores pump parameter data. A laptop with a custom LabVIEW program (National Instruments) and a custom data acquisition system was used to adjust the controller settings and record real-time pump parameters. A microPET R4 scanner (Siemens) with a 1.8 mm spatial resolution at the center of the field of view was used for imaging. All images were reconstructed using 2-dimensional ordered-subsets expectation maximization and analyzed by ASIPro software, with all necessary quality assurance checks and calibrations being performed before imaging.

^{18}F-NaF was synthesized in house. Briefly, ^{18}F-fluoride was diluted with deionized water and passed through a cation-exchange (H^+ form) cartridge and an Accell Plus QMA cartridge (Sep-Pak). The cation cartridge was removed, and the Accell Plus QMA cartridge was rinsed with 10 mL of sterile water and air-dried. ^{18}F-FDG for clinical use was purchased from PETNET Solutions, Inc. The ^{18}F-FDG was used as supplied and required no cation exchange. Both radiotracers were diluted with 5–10 mL of saline and passed through a 0.2 μm filter to provide the end product for imaging. The typical injected activity for PET contrast is 555 MBq (15 mCi). Assuming a typical total blood volume of 5 L for an adult, the concentration needed for the 1.2 L loop was calculated to be 133.2 MBq (3.6 mCi).

The loop was placed in the scanner, with the MVAD® pump positioned in the center of the imaging bore (Fig. 2). The loop reservoir was placed adjacent to the scanner and was surrounded with lead bricks to significantly reduce the contribution of any external radiation to the final imaging counts. The pump was connected to the controller and started. The speed was increased to 14,000 rpm (within the recommended operation range), providing an estimated flow rate of 6.2 L/min. After a 5 min circulation time with no radiopharmaceutical present, the PET scanner acquired a baseline image set over 10 min. The ^{18}F-NaF radiotracer was then injected into the loop. After a 5 min circulation time to achieve a homogeneous mixture, 10 min of imaging was initiated. After the imaging acquisition was complete, the pump was stopped. The loop was dismantled and drained. The loop was rinsed with deionized water, and a post-PET scan (10 min) was then conducted with no solution in the loop and the pump off. This process was repeated for the ^{18}F-FDG radiotracer in a second loop.

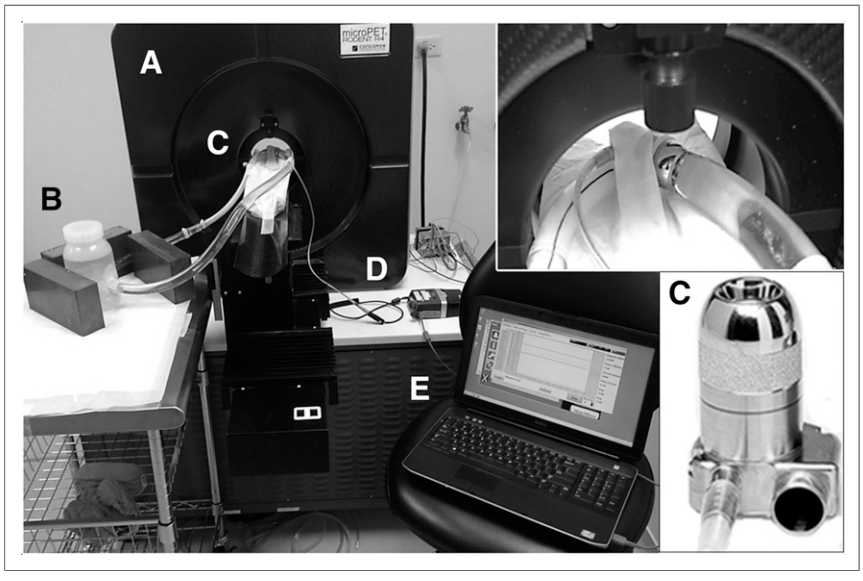

FIGURE 2. Experimental setup: microPET R4 scanner (A), 1.2-L in vitro flow loop with lead bricks shielding loop reservoir (B), MVAD® pump (C), controller connected to MVAD® pump through driveshaft (D), and custom data acquisition system used to capture pump operational parameters (E).

TABLE 1
Pump Parameters for ^{18}F-NaF and ^{18}F-FDG at Baseline and During Radiotracer Circulation

	Baseline			During circulation		
Radiotracer	Power consumption (W)	Flow rate (L/min)	Speed (rpm)	Power consumption (W)	Flow rate (L/min)	Speed (rpm)
^{18}F-NaF	5.39 ± 0.02	6.16 ± 0.00	14,999 ± 3	5.37 ± 0.02	6.16 ± 0.00	14,999 ± 3
^{18}F-FDG	5.19 ± 0.02	6.16 ± 0.00	14,999 ± 3	5.19 ± 0.02	6.16 ± 0.00	14,999 ± 3

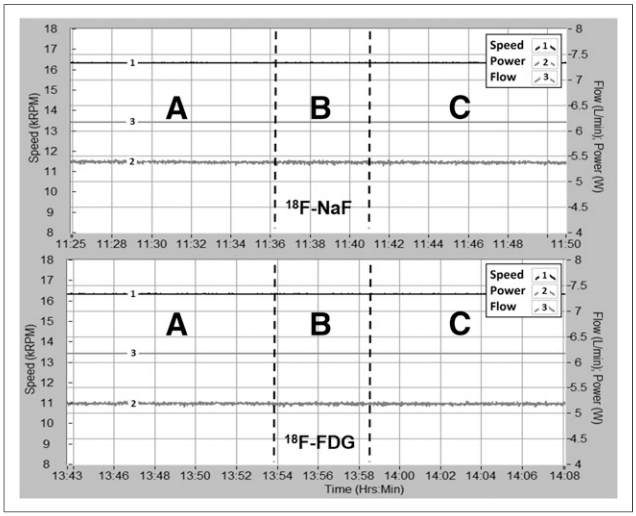

FIGURE 3. Real-time pump parameters: speed, power consumption, and flow rate with ^{18}F-NaF and ^{18}F-FDG. The 3 indicated regions are baseline pump operation (A), introduction and circulation of radiotracer (B), and PET imaging (C).

The reconstructed images were analyzed using ASIPro software. Regions of interest in the full field of view were manually drawn over the images, and the mean voxel values of the counts were determined. The net activity of each PET radiopharmaceutical in the scan was determined by summing the activity in consecutive coronal slices. The mean, SD, minimum, and maximum of the total radioactivity were computed and summarized for each scan. The pump parameters, including power consumption, speed, and estimated flow rate, at 50 Hz were determined and statistically analyzed with Minitab 15. The parameters at baseline were compared with those during and after circulation of the radiotracers.

RESULTS

This study showed PET scanning to have no operational effect on the MVAD® pump during or after circulation of either radiopharmaceutical. Minimal changes in power consumption (W) were observed, with virtually no change in speed (rpm) or estimated flow rate (L/min) between the baseline and circulation conditions (Table 1). There was no statistically significant difference in pump parameters between the baseline and circulation conditions or between the ^{18}F-FDG and ^{18}F-NaF radiotracers (all P values $\geq$ 0.27). Data for the real-time parameters during the ^{18}F-FDG and ^{18}F-NaF loop studies are presented in Figure 3. Controller log files downloaded after the studies revealed no alarms or events triggered during pump operation. Battery power consumption and discharge rates were linear, with no abnormalities.

Each PET scan consisted of 64 slices, with images of the pump limited to only 30–40 of these slices. The regions of interest were drawn over the areas in these slices that showed the pump. Table 2 provides the total radioactivity during radiotracer circulation and after drainage of the loop for both ^{18}F-NaF and ^{18}F-FDG. The mean residual radioactivity was less than 1% for both radiotracers after circulation and drainage of the loop. Imaging of the pump during radiotracer circulation showed minimal artifacts. Figures 4 and 5 provide cross-sectional and 3-dimensional composite images taken during circulation of each radiotracer. The images showed clear flow paths for the inflow, outflow, and volute portions of the pump. Imaging was obscured at the portion of the pump where the impeller was spinning inside the motor core (Fig. 6).

DISCUSSION

The primary finding of this study was that there was no interaction between the radiotracers or PET imaging process and the operation of the MVAD® pump, controller, or battery. No electrical components are housed inside the pump, which contains only the stator core and the wires of the driveshaft connecting the motor to the controller. The

TABLE 2
Total Radioactivity During and After Radiotracer Circulation

	During		After		
Radiotracer	Mean ± SD	Maximum	Mean ± SD	Maximum	Retention
^{18}F-NaF	587.1 ± 772.9	3,184.9	1.8 ± 5.1	101.0	0.31%
^{18}F-FDG	627.6 ± 802.3	3,122.2	3.8 ± 7.9	93.1	0.61%

Data are nCi/mL (1 nCi = 37 Bq).

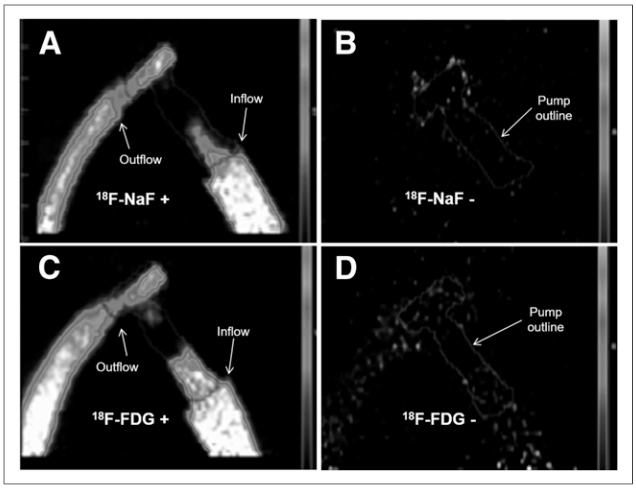

FIGURE 4. Cross-sectional PET images of MVAD® pump during circulation of ^{18}F-NaF (A) and ^{18}F-FDG (C) and after loops were drained to determine the amount of residual ^{18}F-NaF (B) and ^{18}F-FDG (D).

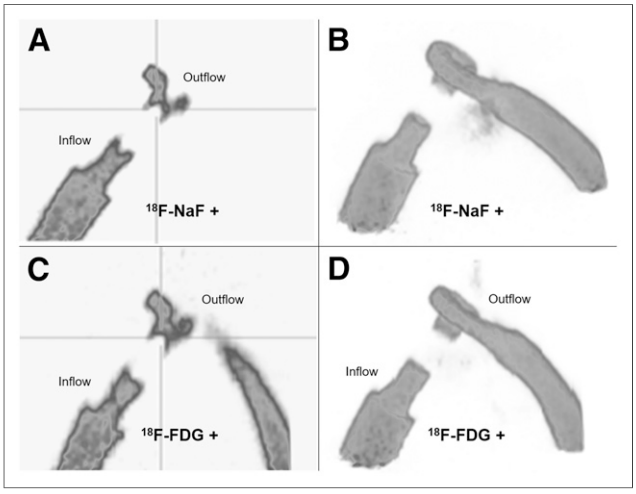

FIGURE 5. Cross-sectional PET images of MVAD® pump during circulation of ^{18}F-NaF (A) and ^{18}F-FDG (C). Three-dimensional reconstruction of PET images obtained during circulation of ^{18}F-NaF (B) and ^{18}F-FDG (D).

housing of the pump is made of a titanium alloy and ceramic, and the impeller is made of magnetized platinum cobalt (*4,5*). With no sensitive electrical components inside the pump, there is significantly less risk of interference or pump failure. The controller contains the microprocessors that operate the pump, manage power, and store diagnostic information. Although the controller may be susceptible to radiation damage, it is not in the direct path of treatment. In addition, because it is external to the body, it can be replaced with a backup if a damaged component causes it to fail.

The secondary findings of this study regard image quality and retention of radiotracers inside the pump. Our previous testing of x-ray and proton radiation therapies on the HVAD pump (a pump that is currently commercially available from HeartWare®, Inc.) showed scattering and attenuation on the images (*16,17*). PET imaging in the current study clearly showed the inflow and outflow regions of the pump; only the portion of the pump with the spinning impeller was obscured (Fig. 6). It is unknown why imaging was not possible in this area, though the cause is likely related to the small radial gaps and high velocity of flow through the impeller (8,000–18,000 rpm). The residual radioactivity after completion of imaging was minimal and expected. It is important that radiotracers not have an affinity for the pump and that they be taken up by the targeted body tissue instead of by the pump components. Less than 1% of the radiotracers were retained after circulation, and because of their short half-life, this residual amount will be gone within a short time.

Application of PET scanning to direct imaging of a VAD has been limited to studies of the detection of VAD-related infections (*1,13–15*). These studies demonstrated increased cell metabolism in areas that have VAD-related infections at the exit site of the driveshaft and at the extremity of the outflow cannula. PET may allow for early detection of infection as well as early evaluation of treatment response. Infection is a significant source of adverse events and a major limitation to

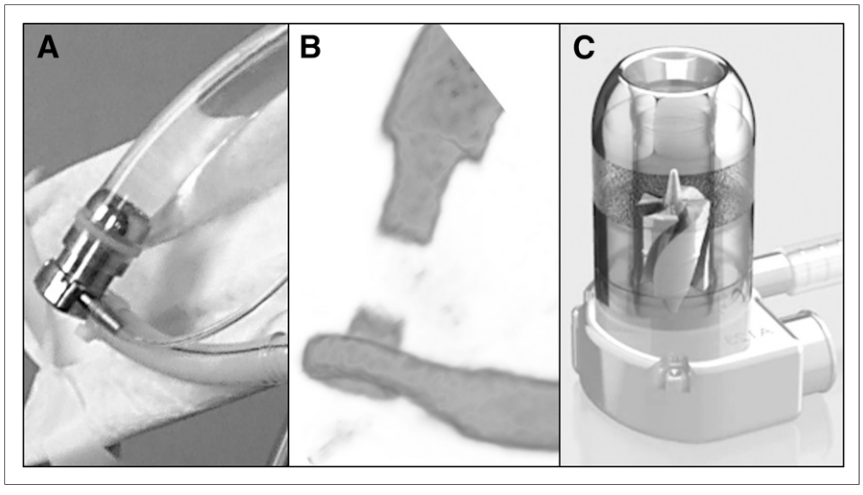

FIGURE 6. (A) MVAD® pump with outflow graft connected to loop. (B) Three-dimensional reconstruction of PET image of circulating radiotracer. Image is obscured in region of pump where impeller is spinning at 14,000 rpm. (C) MVAD® pump showing location of suspended spinning impeller.

further expansion of VAD therapies, but the use of PET may not be exclusive to infections. Another potential use is the detection of a pump-related thrombus inside the pump, inflow cannula, or outflow graft. PET has also been used to detect and determine the age of deep vein thrombosis (*1,18*)—an application that may be useful in the VAD population to determine the location (inflow vs. outflow), size, and age of a thrombus. Further testing will be needed to determine the feasibility of this application.

CONCLUSION

The use of VAD implantation continues to grow as transplantation rates remain constant and the population of heart failure patients increases. Therapies and diagnostic evaluations routinely used in hospitals need to be reviewed for use in VAD patients. Potential interactions between the life-sustaining devices and therapies must be carefully considered in order to decrease the risk of inaccurate diagnostics (imaging), incomplete treatment delivery, or pump failure. PET may have additional utility outside its current use, detection of infection. In this in vitro study, no interaction was observed between the MVAD® pump and direct PET imaging with two commonly used radiotracers. Clear imaging of the internal pump components was possible, with minimal radiotracer retention in the pump components after circulation.

DISCLOSURE

No potential conflict of interest relevant to this article was reported.

REFERENCES

1. Dembitsky WP, Tector AJ, Park S, et al. Left ventricular assist device performance with long-term circulatory support: lessons from the REMATCH trial. *Ann Thorac Surg.* 2004;78:2123–2129.
2. Wohlschlaeger J, Schmitz KJ, Schmid C, et al. Reverse remodeling following insertion of left ventricular assist devices (LVAD): a review of the morphological and molecular changes. *Cardiovasc Res.* 2005;68:376–386.
3. Tuzun E, Roberts K, Cohn W, et al. In vivo evaluation of the HeartWare centrifugal ventricular assist device. *Tex Heart Inst J.* 2007;34:406–411.
4. Slaughter MS, Giridharan GA, Tamez D, et al. Transapical miniaturized ventricular assist device: design and initial testing. *J Thorac Cardiovasc Surg.* 2011;142:668–674.
5. McGee E Jr, Chorpenning K, Brown MC, et al. In vivo evaluation of the HeartWare MVAD. *J Heart Lung Transplant.* 2014;33:366–371.
6. Popov AF, Hosseini MT, Zych B, et al. Clinical experience with HeartWare left ventricular assist device in patients with end stage heart failure. *Ann Thorac Surg.* 2012;93:810–815.
7. Wilson SR, Givertz MM, Garrick CS, Stewart C, Mudge GH. Ventricular assist devices: the challenge of outpatient management. *J Am Coll Cardiol.* 2009;54:1647–1659.
8. Slaughter MS, Sobieskii MA, Tamez D, et al. HeartWare miniature axial-flow ventricular assist device: design and initial feasibility test. *Tex Heart Inst J.* 2009;36:12–16.
9. Deuse T, Reichenspurner H. Do not touch the sternum-thoracotomy incisions for HVAD implantation. *ASAIO J.* 2014;60:234–236.
10. Sileshi B, Haglund NA, Davis ME, et al. In-hospital outcomes of a minimally invasive off-pump left thoracotomy approach using a centrifugal continuous-flow left ventricular assist device. *J Heart Lung Transplant.* 2015;34:107–112.
11. Tai YF, Piccini P. Applications of positron emission tomography (PET) in neurology. *J Neurol Neurosurg Psychiatry.* 2004;75:669–676.
12. Duhaylongsod FG, Lowe VJ, Patz EF, et al. Detection of primary and recurrent lung cancer by means of F-18 fluorodeoxyglucose positron emission tomography (FDG PET). *J Thorac Cardiovasc Surg.* 1995;110:130–139.
13. Costo S, Hourna E, Massetti M, et al. Impact of F-18 FDG PET-CT for the diagnosis and management of infection in JARVIK 2000 Device. *Clin Nucl Med.* 2011;36:e188–e191.
14. Tlili G, Picard F, Pinaquy JB, et al. The usefulness of FDG PET/CT imaging in suspicion of LVAD infection. *J Nucl Cardiol.* 2014;21:845–848.
15. Kim J, Feller ED, Chen W, Dilsizian V. FDG PET/CT imaging for LVAD associated infections. *JACC Cardiovasc Imaging.* 2014;7:839–842.
16. Gossman MS, Graham JD, Tamez D, et al. Evaluation of a ventricular assist device: stability under x-rays and therapeutic beam attenuation. *ASAIO J.* 2012;58:212–216.
17. Gossman MS, Graham JD, Das IJ, et al. Evaluation of a ventricular assist device system: stability in a proton beam therapy. *ASAIO J.* 2012;58:597–600.
18. Rondina MT, Lam UT, Pendleton RC, et al. F-FDG PET in the evaluation of acuity of deep vein thrombosis. *Clin Nucl Med.* 2012;37:1139–1145.